Dynamics near free surfaces of molecular dynamics simulated $Ni_{0.5}Zr_{0.5}$ metallic glass films

B. Böddeker* and H. Teichler†
Institut für Materialphysik and Sonderforschungsbereich 345, Universität Göttingen, Hospitalistrasse 3/7, D-37073 Göttingen, Germany
(Received 20 August 1998)

Results are reported from molecular dynamics simulations of glass forming films with $Ni_{0.5}Zr_{0.5}$ adapted potentials, which show a dramatic enhancement of the dynamics near the surface. After relaxation of the film for 10^{-8}–10^{-7} s, the dynamics is investigated by a spatially resolved effective diffusion constant and by the decay rates of Ni-Zr next-neighbor bonds. At the simulated bulk glass transition temperature, the atomic mobility varies across the film by more than two orders of magnitude from that of a liquid at the film surface to bulk values of an arrested solid in the interior. This variation of the dynamics is also observed slightly above and below the glass transition. Despite the large variation in the atomic mobility, an analysis of the van Hove correlation functions indicates a global dynamic glass transition, common to the surface and core of the film. The decrease of the mobility with depth is exponential, with a smooth transition between surface and bulk behavior. A Landau analysis is applied to interpret the spatial dependence of the mobility, using a hidden parameter, possibly related to the time scale of the fluctuations in the system. The decay length and surface excess mobility, corresponding to the exponential decrease, are only slightly temperature dependent, without a singularity at the glass transition. Analogies of this phenomenon to the dynamics of confined glass forming liquids and to the surface melting of metallic crystals are discussed. [S1063-651X(99)02502-7]

PACS number(s): 64.70.Pf, 68.60.−p, 68.45.Gd, 68.15.+e

I. INTRODUCTION

In several cases, it is well known that the surface of a solid or liquid alters the dynamics of the material in the surface region: First, there are the phenomena of surface melting (SM) of crystals [1–6] and the melting point depression of confined liquids [7,8]. These observations can be explained by thermodynamic arguments on the assumption that the liquid phase has a smaller surface free enthalpy than the solid but a higher volume free enthalpy. Second, there are experiments on glass forming liquids that show under confinement, e.g., a shift of the glass transition temperature and a change in the viscosity or in the rotational dynamics (for a review, see Refs. [9–11]). These observations are, however, rather controversial and no unifying theoretical description exists so far explaining these results.

The present contribution reports a different but probably related phenomenon, namely, a marked increase in the dynamics of a metallic glass and the related highly viscous, undercooled melts in a region below a free surface to the vacuum. Our results are deduced from molecular dynamics (MD) simulations of an amorphous $Ni_{0.5}Zr_{0.5}$ metallic film, where the described phenomena appear after relaxations of the structure for 10^{-8}–10^{-7} s.

Surface melting (SM) of crystals is defined by the presence of liquidlike layers on the surface of a crystalline solid at temperatures well below the bulk melting temperature T_m. The phenomenon is well known for ice [5,6] and metal surfaces [1] (see also Refs. in Ref. [2]). MD simulations [2–4] proved particularly helpful in promoting our knowledge in this field. They yield, in broad agreement with the experiments, that the (110) surfaces of Pb, Al, Cu, Au, and Ni display SM, whereas the (111) surfaces remain stable at all temperatures below T_m. One interpretation of SM assumes that the relatively high volume free enthalpy of the liquid surface layer on the crystal may be compensated by a reduction of the surface free enthalpy. While the undercooled liquid is metastable in the bulk, it may become stable at the surface [6]. For short range potentials as those used for the simulations in this work, a Landau theory [12] predicts a logarithmic divergence of the thickness of the liquid surface layer as T_m is approached from below.

Assuming a phenomenon of similarly increased mobility near the free surface of a (metallic) glass, there would be fundamental differences to the SM of crystals. The glass itself is a metastable thermodynamic state and is only realized while the entrance into the stable crystalline phase is suppressed by kinetic hindrances. Thus, equilibrium thermodynamics do not apply. One might adopt the view that the system takes on the most favorable of the accessible metastable states, a picture used successfully to construct metastable phase diagrams including the glass state or to interpret solid state amorphization reactions and inverse melting [13,14]. However, a further difference comes from the absence of a distinct structural transition between the undercooled liquid and the glass. In the case of glass surfaces, we therefore do not expect a marked boundary in the structure between the surface layer with its liquidlike mobility and the bulk glass. But, as the liquid-glass transition is a dynamical one [15], a transition is expected in the fluctuation dynamics on a spatial scale. In contrast to the SM of crystals, the thickness of the liquidlike surface layer of the metallic glass, investigated in this work, shows no divergence in the glass transition temperature range. It has a finite thickness at temperatures slightly above and below the glass transition.

A large number of experimental studies considers the effects of spatial confinement on glass forming molecular liquids (for review, see Refs. [9–11]). The liquids can be con-

*Electronic address: bboedde@gwdg.de
†Electronic address: teichler@umpa06.gwdg.de

fined in micro porous materials or as droplets in microemulsions [16], hydrogels [17], or butyl rubber [18]. These systems with high internal surface-to-volume ratio allow to measure the influence of confinement on dielectric properties and on T_G. The dielectric measurements reflect the rotational dynamics of the liquid molecules. A lower surface-to-volume ratio has the geometry of liquids confined between parallel plates. But this arrangement allows the direct measurement of the viscosity by the response to shear forces [22].

One of the most widely accepted concepts for the interpretation of the results and a concept for the glass transition itself is that of the correlation length ζ of cooperativity [18,19]. ζ is assumed to increase with decreasing temperature and to diverge at a temperature T_0 below T_G. The length scale of confinement at which the first deviation of the dynamic properties to those of the bulk occurs should then be proportional to ζ.

In some cases, the dynamics seems to increase [18–20], in others to decrease [21–23], or not to shift [16,17,23] under the confinement of glass forming liquids. This leads to a decreased or increased T_G, respectively. In the case of confinement by microporous silica glasses, a layer of molecules can permanently be bound to the inner surfaces by hydrogen bonds. This layer has significantly reduced dynamics, which should not be confused with the influence of the confinement on the remaining liquid [24].

The free standing film considered here has the same geometry as the film confined between parallel plates. Direct measurements of the viscosity of an unpolar, globular, vander-Waals-like liquid, confined between atomically smooth crystalline mica plates, displays a smooth slowing down of the dynamics to that of a solid during reduction of the film thickness between 10 and 1 molecular diameters [22]. Computer simulations of simple binary liquids, confined between structureless plates [25], suggest an increase of the critical temperature T_c compared to the bulk. The simulations indicate that the dynamic glass transition is a collective process, which takes place in all layers of the film simultaneously. The decrease of the self diffusion constant with the reduction of the plate distance fits to an exponential function. For polymer films [26–29], experiments on the effect of the free surface have been conducted, showing a decrease of the glass transition temperature T_G with the reduction of film thickness.

The next section will describe the physical models and numerical methods used in our MD simulations. Section III presents the results. The diffusion profile in the amorphous $Ni_{0.5}Zr_{0.5}$ films is discussed. The dynamic glass transition is examined by means of the van Hove correlations. The decay rates of Ni Zr next-neighbor bonds are used as an alternative way to describe the profile of the dynamics in the film. Data on a film grown by deposition are presented. The paper concludes with a summary.

II. MODEL AND METHOD

In our MD simulations, we consider amorphous $Ni_{0.5}Zr_{0.5}$ films of $L_3 = 2.8$ to 4.2 nm thickness. $Ni_{0.5}Zr_{0.5}$ was chosen as it is a metallic glass forming system, well studied by MD simulations [30–40] and experiments [41–43]. In order to model $Ni_{0.5}Zr_{0.5}$ we use two different formulations: a semiempirical one, adapted to the electron theoretical Hausleitner-Hafner [44] approach (HHA) of the interatomic couplings in transition metal glasses, and an ''embedded atom method'' (EAM) approach. The first approach was chosen since we know from our previous studies [30,34–36] various details on the glass transition in this model, which are necessary for interpretation of the current surface and thin film results. The EAM model was included to test, to a certain degree, the independence of our results from the applied interatomic potentials.

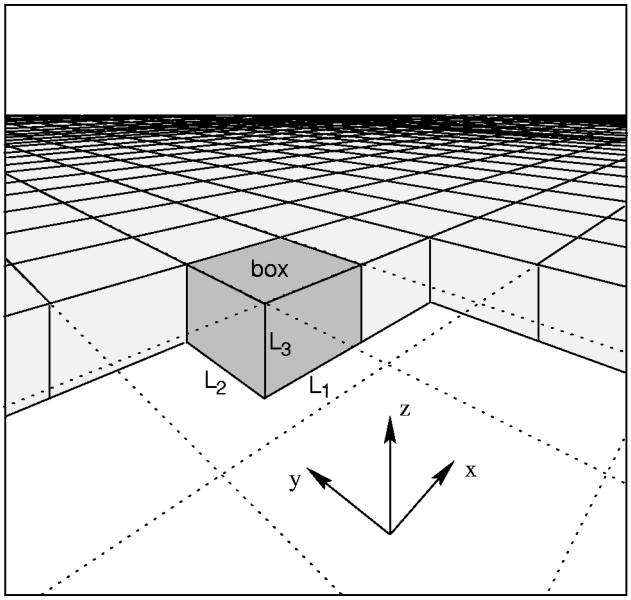

FIG. 1. Schematic plot of the situation under consideration. The film consists of periodic replicas of the simulation box in the x and y directions. The box has the size $L_1 \times L_2 \times L_3$. In the z direction the film has two free surfaces to the vacuum. $z = 0$ is defined to be the bottom surface of the film.

The MD simulations are carried out as isothermal-isochoric/isobaric calculations. The temperature is fixed by suitably scaling the mean kinetic energy. The Newtonian equations of N atoms ($N = 1181$ in the HHA, $N = 1000$ for EAM) are numerically integrated by a fifth-order predictor-corrector algorithm (time step $dt = 2 \times 10^{-15}$ s) in a tetragonal simulation volume with periodic boundary conditions, fixed spatial extensions L_1 and L_2 in the film plane, and variable nonperiodic extension L_3 across the film. This geometry is shown in Fig. 1. The film has two surfaces facing an absolute vacuum. No atoms evaporate during the time of simulation. During the simulation, L_3 is approximated using the mean square distances of the atom positions from the film center. Typically, $L_3 \approx 4.2$ nm in the HHA (2.8 nm in the EAM), while $L_1, L_2 \approx 2.3$ nm in the HHA (2.5 nm in the EAM). The small number of atoms was chosen to facilitate long time simulations over nominally 25 to 50 ns, necessary to generate sufficiently relaxed structures and to analyze their dynamics with sufficient reliability. As described before [30,34–36], our HHA models the interatomic couplings by pair potentials, adapted to the Hausleitner-Hafner potentials [44], and by a global electron density dependent term $E_0(\rho)$, which is taken from Ref. [45], where $\rho \propto (L_1 L_2 L_3)^{-1}$ is estimated by assuming homogeneous particle density and com-

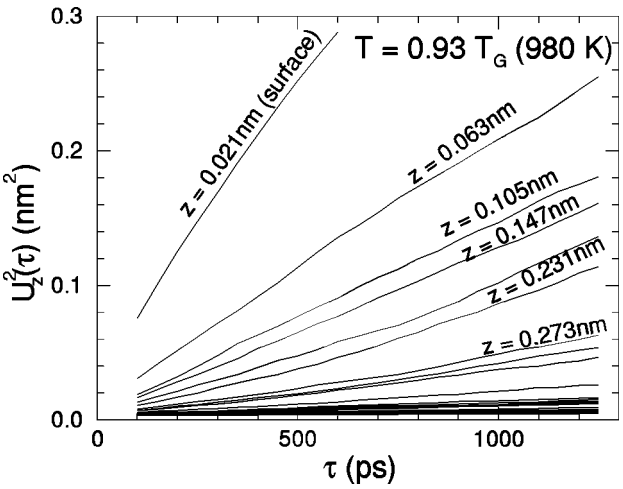

FIG. 2. Atomic mean square displacement curves $U_z^2(\tau)$ for a set of depth values z in the 1100 K HHA-MD-simulated film. The curves are in good approximation linear within the shown time interval of $[\tau_0=100$ ps, $\tau_1=1250$ ps].

position across the film. In the EAM modeling, we use potentials developed by Spangenberg [46] on extending the pure metals results of Oh and Johnson [47] to the alloy system by taking into account the lattice constants, cohesive energies, and bulk moduli of $Ni_{0.5}Zr_{0.5}$ and $Ni_{0.33}Zr_{0.67}$.

III. RESULTS

A. Diffusion

The basic results, deduced from our HHA-MD simulations, are displayed in Fig. 3. The logarithmic ''effective mean diffusion coefficient'' D is shown for four temperatures between 980 and 1160 K as a function of depth z below the top surface for films of 4.2 nm thickness. The films are prepared in the computer by forming suitable tetragonal samples from bulk amorphous 980 and 1060 K material [30], annealing them at the selected four temperatures for approximately 10–25 ns, sufficient to generate relaxed structures with steady-state atomic dynamics, and adding subsequent MD runs over 10–25 ns to record the atomic motions.

The $D(z)$ are evaluated from the atomic displacements $\mathbf{u}_i(\tau,t)=\mathbf{x}_i(t+\tau)-\mathbf{x}_i(t)$. The mean square displacements $U_z^2(\tau)$ are evaluated by grouping the $\mathbf{u}_i^2(\tau,t)$ according to the initial depth $x_{3,i}(t)$ of the atoms and averaging t along the steady-state time evolution of the system:

$$U_z^2(\tau) := \langle \mathbf{u}_i^2(\tau,t)\rangle_{i,t}^z, \tag{1}$$

where $\langle\cdot\rangle_{i,t}^z$ denotes an average over all combinations of time t and atom index i, which comply to the condition $x_{3,i}(t)\approx z$:

$$\langle\cdot\rangle_{i,t}^z = \frac{\langle\cdot\,\delta(z-x_{3,i}(t))\rangle_{i,t}}{\langle\delta(z-x_{3,i}(t))\rangle_{i,t}}. \tag{2}$$

As shown for the 980 K HHA film in Fig. 2, $U_z^2(\tau)$ is approximately linear in the interval $[\tau_0=100$ ps, $\tau_1=1250$ ps]. For short times $\tau\ll\tau_0$, vibrational motions cause a steep increase of $U_z^2(\tau)$. For long times $\tau\gg\tau_1$, vertical motion of the atoms across the film cause a deviation from linearity. $D(z)$ is defined as $\frac{1}{6}$ of the slope of $U_z^2(\tau)$, calculated by linear regression in the interval $[\tau_0=100$ ps, $\tau_1=1250$ ps]:

$$D(z) := \frac{\langle U_z^2(\tau)\ \ (\tau-\langle\tau\rangle)\rangle}{6\langle(\tau-\langle\tau\rangle)^2\rangle}, \tag{3}$$

where $\langle\cdot\rangle$ denotes an average over $\tau\in[\tau_0,\tau_1]$. For homogeneous three-dimensional systems, $D(z)$ turns into the (components averaged) diffusion coefficient in the long time limit $\tau_1\to\infty$.

1. Diffusion in the HHA-MD-simulated films

The curves in Fig. 3 show a marked decrease in $D(z)$ with increasing distance from the film surface on both sides of the film, until a constant bulk value $D(\infty)$ in the interior is reached. $D(z)$ can be well approximated by

$$D(z)=D(\infty)(1+qe^{-z/z_0}), \tag{4}$$

with

$$q=\frac{D(0)}{D(\infty)}-1, \tag{5}$$

where z measures the distance from the surface and is limited to half the film thickness.

Fits of Eq. (4) are included in Fig. 3, and the corresponding parameters are displayed in Table I.

For the interpretation of these findings, they are compared with the results from simulated bulk material of the same $Ni_{0.5}Zr_{0.5}$ model under similar thermal conditions [34,35,30]. The bulk simulation yields a caloric glass transition temperature $T_G=1050$ K [35] and a critical temperature $T_c=1120$ K [34,35]. According to the mode coupling theory [15] of the liquid-glass transition, T_c separates the regimes of dominating liquid flow dynamics and of atomic hopping motion. Furthermore, simulated diffusion data were recently provided [30] for the present model. They indicate for mid-concentration composition that the Ni and Zr diffusion coefficients have a common T_c, above which they differ by a factor of 2–3. In Fig. 4, the composition averaged bulk diffusion coefficients [35], governed by the Ni diffusion, are displayed. They follow the critical law $|T-T_c|^\gamma$, with non-universal exponent γ, as predicted by the mode coupling theory [15]. Below T_G, an Arrhenius behavior is found [30]. For the more mobile Ni-atoms, the activation energy and pre-exponential factor are in close agreement with experimental data [48]. The estimated values for $D(\infty)$ in the core region of the simulated films agree well with the composition averaged diffusion coefficients in the bulk system [30] at the same temperatures (see Fig. 4), supporting the view that the interior of the film behaves like bulk material. The surface values $D(0)$, also presented in Fig. 4, correspond to simulated diffusion coefficients in the melt between 1300 and 1400 K. In the surface sheet, the decrease of the effective diffusion coefficients with depth z towards the bulk value is exponential, with decay length z_0. The decay length changes smoothly with the temperature in the investigated temperature range, including T_G and T_c.

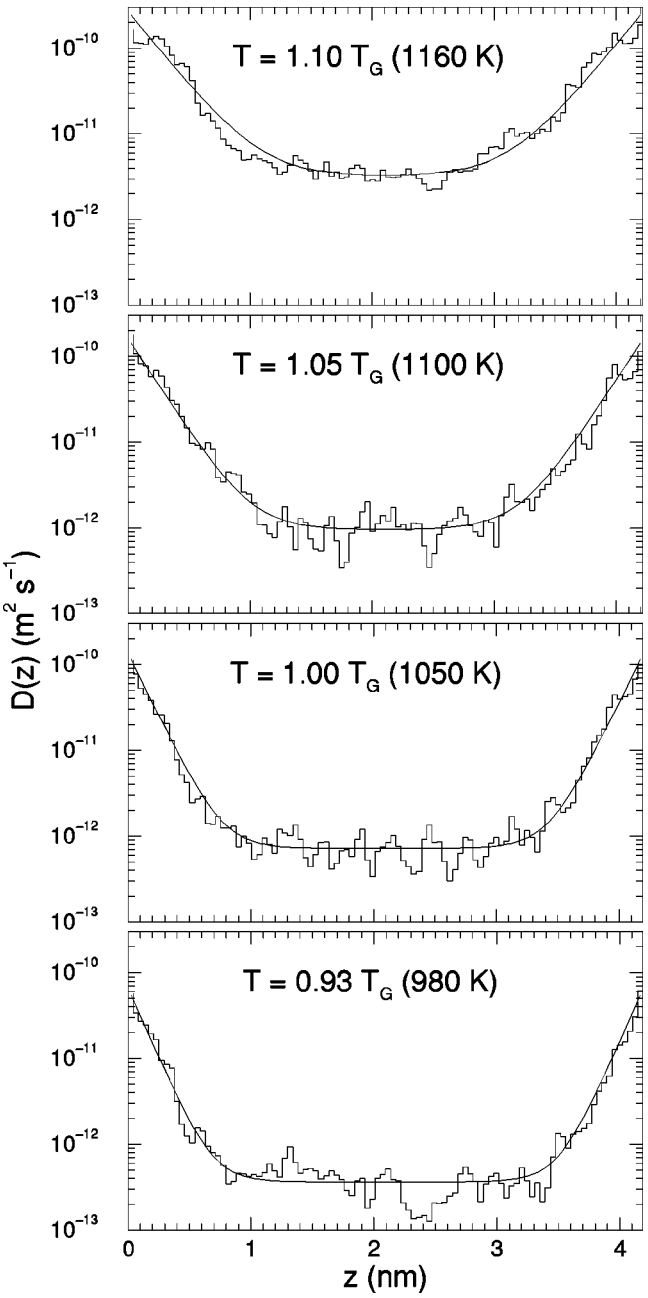

FIG. 3. Effective diffusion profiles in the $Ni_{0.5}Zr_{0.5}$ film for several temperatures near the glass transition. Each plot shows the logarithmic effective mean diffusion coefficient $D(z)$ as a function of depth z in the film, with surfaces to the vacuum at $z=0$ nm and $z\approx 4.2$ nm. The exponential increase of $D(z)$ near the surface gets steeper and higher with decreasing temperature. [Stair steps: data taken from the HHA-MD simulations. Smooth curves: least-mean-square fits of the analytical expression Eq. (4).]

2. Diffusion in the EAM-MD-simulated films

Figure 5 provides $D(z)$ data from MD-simulations with the described EAM potentials. The film is treated similarly as the HHA-simulated film. When comparing these data with the HHA results, one has to take into account that the present EAM description yields a T_G of approximately 980 K. With this in mind, we find rather fair agreement between the predictions about the surface dynamics from both models. The flat portion in $D(z)$ near the surface is due to an enrichment of the less mobile Zr atoms in the outer surface layer. A side result can be extracted from the fact that the gradient of the diffusion coefficients forms at 1080 K, even though the total film thickness seems smaller than the extent of the surface layers. This confirms that the observed phenomenon is not based on a boundary between a bulklike core phase and a surface phase.

TABLE I. Parameters for the asymptotic description Eq. (4) of the effective mean diffusion coefficients $D(z)$ in the HHA-MD simulations. [$D(\infty)$ in units $\mu m^2\,s^{-1}$.]

T (K)	z_0 (nm)	q	$D(\infty)$
980	0.13	180	0.36
1050	0.15	180	0.72
1100	0.20	170	0.95
1160	0.25	81	3.17

3. Crystallization

The data in Fig. 3 cover a temperature range between 1160 and 980 K, which includes the estimated T_c and T_G [34]. At higher temperatures we observe crystallization of the film within annealing times of 10 ns, a time scale where crystal nucleation is not observed in simulations of the bulk material. Also, the 1160 K sample tends to crystallize under further annealing beyond the limit of 20 ns, which are taken into account in the construction of the corresponding curve in Fig. 3. Hence, the crystallization temperature T_X of the film is below 1160 K. At 1100 K and below, crystallization was not observed within 50 ns annealing time. Below T_G, crystallization is not expected to take place in samples of sufficient thickness. Since crystallization proceeds very fast after the nucleation, it can reliably be distinguished from the phenomenon explored in this paper.

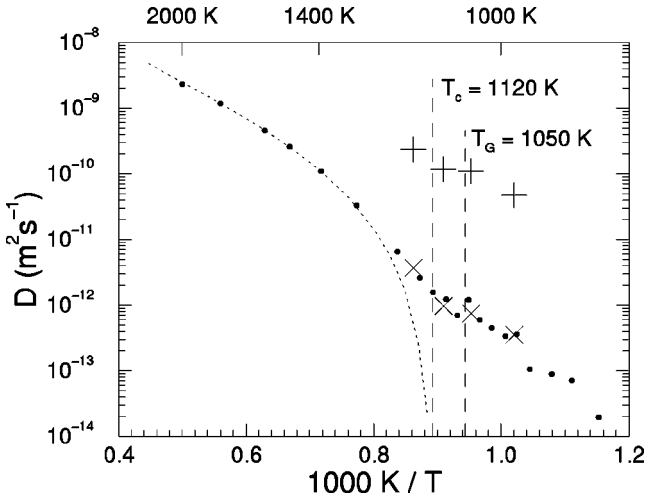

FIG. 4. Arrhenius plot of the composition averaged diffusion coefficients from HHA-MD simulations: The diffusion coefficients of the bulk material (dots) are taken from the HHA-MD-simulations in Ref. [30]. Above $T_c=1120$ K they follow a power law (dotted line). The effective diffusion coefficients in the core region of the films [$D(\infty)$, symbol: $\times$] agree well with the bulk values. The effective diffusion coefficients at the surface of the film [$D(0)$, symbol: $+$] reach values of the bulk melt of higher temperatures.

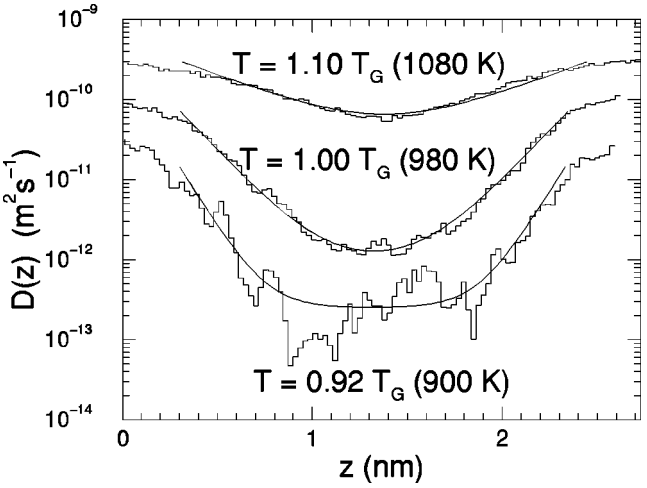

FIG. 5. Same representation of effective diffusion profiles $D(z)$ for several temperatures near the glass transition as in Fig. 3, but with data from the EAM-MD-simulated film. The increase of the $D(z)$ curves near the surface gets steeper and higher with decreasing temperature. The flat regions of $D(z)$ at the surfaces are due to surface layers of the less mobile Zr atoms in the simulation of this EAM model. The film thickness is so small that no region with constant $D(z)$ forms in the center of the film at 1080 K. The gradient of $D(z)$ appears nevertheless.

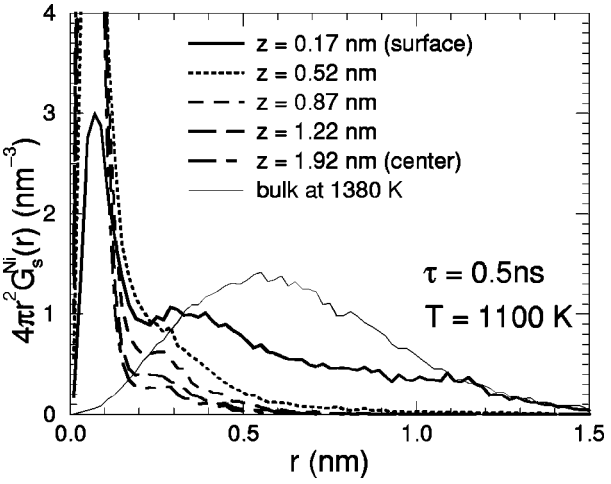

FIG. 6. Angular averaged self part of the van Hove correlation function $4\pi r^2 G_s^{\mathrm{Ni}}(r,\tau=500\ \mathrm{ps})$ for the Ni atoms in HHA-simulated material. The bold curves are taken from several depths z in the HHA-MD-simulated film at $T=1100$ K, just below the bulk $T_c=1120$ K. The humps near $r=0.3$ nm indicate the presence of hopping processes in all depths (including the surface). $4\pi r^2 G_s^{\mathrm{Ni}}(r,\tau=500\ \mathrm{ps})$ is also included for the bulk liquid at 1380 K (thin line). The bulk liquid at 1380 K has the same diffusion constant as the film surface at 1100 K. In this case, $G_s^{\mathrm{Ni}}(r,\tau=500$ ps) has the smooth Gaussian form at 1380 K expected for purely viscous matter transport.

B. van Hove and pair correlations

We further analyzed the dynamic glass transition regarding a possible spatial inhomogeneity of this transition. During the dynamic glass transition, the mode of transport changes from the viscous flow of the liquid to hopping motion. At the critical temperature T_c, both processes are approximately in balance. A tool to analyze the motion is the self part of the angular averaged van Hove correlation function $G_s(r,\tau)$. $4\pi r^2 G_s(r,\tau)$ describes the probability distribution of distances between the atoms and their original positions after a time evolution of length τ. In case of liquid, viscous flow, $G_s(r,\tau)$ has a simple Gaussian form, broadening with $\sqrt{\tau}$. In case of hopping processes at intermediate times τ, sharp peaks arise at discrete distance values of neighbored places.

The HHA-simulated film is analyzed at 1100 K, just below the bulk $T_c=1120$ K. Figure 6 shows an array of $G_s^{\mathrm{Ni}}(r,\tau=500\ \mathrm{ps};z)$ curves of the Ni atoms in several depths z of this film. The time interval τ is fixed to 500 ps. The angular averaged self part of the van Hove correlation function for the Ni atoms in the depth z is calculated by

$$4\pi r^2 G_s^{\mathrm{Ni}}(r,\tau;z)=\langle \delta(r-\|\mathbf{x}_i(t)-\mathbf{x}_i(t+\tau)\|)\rangle^z_{i\in \mathrm{Ni},t}, \quad (6)$$

where $\langle\cdot\rangle^z_{i\in \mathrm{Ni},t}$ denotes an average over time t, and Ni atoms i, with $x_{3,i}(t)\approx z$ analogous to Eq. (2). Figure 6 also includes $4\pi r^2 G_s^{\mathrm{Ni}}(r,\tau=500\ \mathrm{ps})$ of the bulk HHA-MD-simulated liquid at 1380 K (thin line). At this temperature, the bulk diffusion coefficient approximately equals the effective diffusion $D(0)$ at the surface of the 1100 K film. $G_s^{\mathrm{Ni}}(r,\tau=500$ ps) of the bulk liquid agrees with the smooth Gaussian form expected for the viscous flow [shown is $G_s^{\mathrm{Ni}}(r,\tau=500$ ps) multiplied by $4\pi r^2$]. The $G_s^{\mathrm{Ni}}(r,\tau=500\ \mathrm{ps};z)$ curves of the film deviate significantly from the Gaussian behavior at all depths. $4\pi r^2 G_s^{\mathrm{Ni}}(r,\tau=500\ \mathrm{ps};z)$ is structured with a first maximum at approximately 0.1 nm, a first minimum at approximately 0.2 nm, and the onset of one or more additional maxima. Thus, the hopping diffusion mechanism of the glass is relevant for the complete film at 1100 K, just below the bulk T_c. In spite of its liquidlike effective diffusion coefficients, even the surface layer should be viewed as a dynamic glass at 1100 K. This leads to the conclusion that the dynamic glass transition in this metallic film is a collective phenomenon, taking place in all layers simultaneously between 1100 K and the bulk T_c of 1120 K. This is in agreement with an observation in a soft sphere model of confined glass forming liquids where the dynamic glass transition is found in all layers of the film simultaneously [25].

Figure 7 presents the angular averaged partial pair correlation functions $g_{ij}(r)$ for the HHA-simulated bulk glass at 980 K and for the atoms in the interior of the film at the same temperature. It demonstrates the close similarity of the data and further supports the notion that the interior of the film corresponds to bulk material.

C. Dynamics of next neighbor bonds

In this section, the decay rates $\nu_{\mathrm{NiZr}}(z)$ of the Ni-Zr next-neighbor bonds shall be considered as an alternative way to describe the dynamics in the film. Such an approach was used in Ref. [36] to study the temperature dependence of the configuration dynamics. Here it is used to uncover the spatial structure of the atomic dynamics.

The approach makes use of correlation functions which describe the probability of finding two atoms as nearest neighbors at time $t+\tau$, after they have been nearest neighbors at time t. A pair of Ni and Zr atoms is defined as a

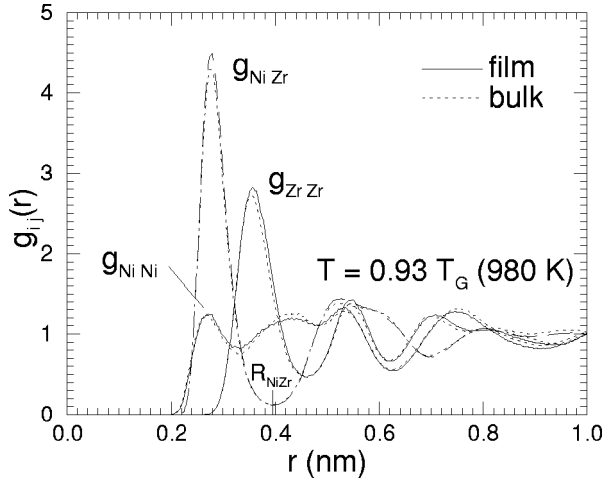

FIG. 7. Angular averaged partial pair correlation functions $g_{ij}(r)$, from HHA simulations at 980 K. There is a close similarity between the data from the core of a film (dotted line) and from bulk material treated similarly. A deep minimum of $g_{\mathrm{NiZr}}(r)$ at $R_{\mathrm{NiZr}}=0.395$ nm indicates that the first NiZr neighborhood shell is well separated from the following shells.

nearest-neighbor pair, when the atoms have a distance less than R_{NiZr}, where $R_{\mathrm{NiZr}}=0.395$ nm is the position of the first minimum in $g_{\mathrm{NiZr}}(r)$ (see Fig. 7). This is expressed in $b(i,j,t)$, being 1 when Ni atom i is a neighbor of Zr atom j at time t and 0 otherwise:

$$b(i,j,t)=\Theta(R_{\mathrm{NiZr}}-\|\mathbf{x}_i(t)-\mathbf{x}_j(t)\|), \tag{7}$$

where Θ denotes the Heaviside step function. Figure 8 displays the autocorrelation functions $\Phi(\tau;z)$ of the Ni Zr bonds for slices with depth z in the film:

$$\Phi(\tau,z)=\frac{\langle b(i,j,t)b(i,j,t+\tau)\rangle^{z}_{i\in\mathrm{Ni},j\in\mathrm{Zr},t}}{[\langle b(i,j,t)\rangle^{z}_{i\in\mathrm{Ni},j\in\mathrm{Zr},t}]^2}, \tag{8}$$

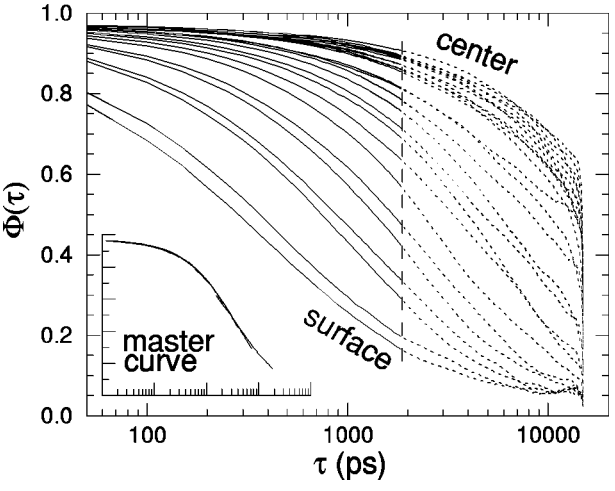

FIG. 8. Autocorrelation functions $\Phi(\tau,z)$ for Ni-Zr bonds at different depths in the HHA-MD-simulated film at 1100 K. Due to the low statistics of the dotted parts, only the solid parts of the curves are included in the master curve (inset) by a shift on the logarithmic time scale. The decay rates $\nu_{\mathrm{NiZr}}(z)$ in Fig. 9 are calculated from this shift.

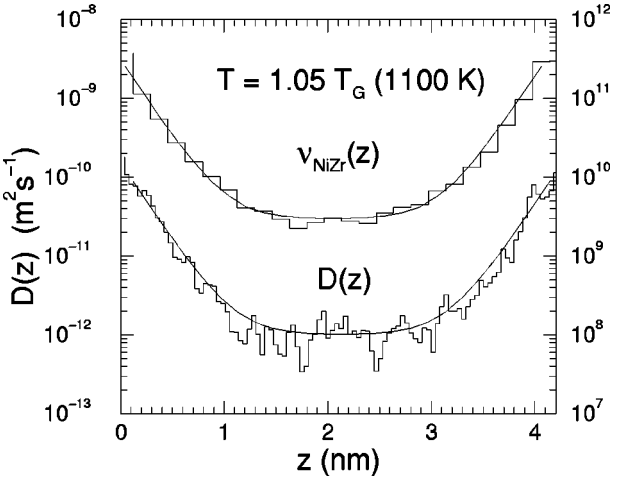

FIG. 9. Mobility profile in the HHA-MD-simulated film, described by the diffusion $D(z)$ and the decay rate of the NiZr next-neighbor bonds $\nu_{\mathrm{NiZr}}(z)$ (stair steps). The smooth curves represent a fit to Eq. (4) with values $z_0=73$ and $q=0.01$ for both curves.

where $\langle\cdot\rangle^{z}_{i\in\mathrm{Ni},j\in\mathrm{Zr},t}$ denotes an average over time t, Ni atoms i, and Zr atoms j, with $[x_{3,i}(t)+x_{3,j}(t)]/2\approx z$ analogous to Eq. (2).

By shifting the curves $\Phi(\tau;z)$ on a logarithmic time scale, they fit onto a common master curve, as shown in the inset of Fig. 8. The shift of $\Phi(\tau;z)$ onto the master curve yields, up to a common factor, the life time of the Ni-Zr bonds in each slice z. The decay rates $\nu_{\mathrm{NiZr}}(z)$ in Fig. 9 are the inverse lifetimes. They can be fitted to the same functional form [Eq. (4)] as $D(z)$. In Fig. 9 the same decay length z_0 and excess q of the dynamics at the surface are used for both numerical fits. $D(z)$ and $\nu_{\mathrm{NiZr}}(z)$ show the same dependence on z.

D. Landau analysis

The exponential decrease [Eq. (4)] of $D(z)$ and $\nu_{\mathrm{NiZr}}(z)$ near the surface indicates a hidden parameter in the system, which induces spatially varying dynamics. Careful analysis of the structure shows that there are no significant changes in the density nor in the chemical compositions on the relevant length scale of 1 nm below the surface. Thus, the hidden parameter reflects a more sophisticated quantity, most probably related to the time scale of the fluctuations in the system. If one relies on the free volume picture, the hidden parameter probably describes the time scale of free volume fluctuations. Here it is assumed that the influence of the parameter can be taken into account by a state parameter $\Psi_0(z)$, which scales the mobility, i.e.,

$$D(z)=D(\infty)\Psi_0(z). \tag{9}$$

Following the Landau formalism, the spatial shape of $\Psi_0(z)$ shall take a form that minimizes a hypothetical energy functional [49],

$$K(\{\Psi\})=\int dz[\tfrac{1}{2}z_0^2|\partial_z\Psi(z)|^2+W(\Psi(z)) +z_0\delta(z)W_s(\Psi(z))]. \tag{10}$$

The diffusive contribution

$$z_0^2|\partial_z\Psi(z)|^2$$

keeps $\Psi_0(z)$ smooth. The surface energy

$$W_s(\Psi(0))=-q\Psi(0)$$

fixes $\partial_z\Psi_0(0)=-(q/z_0)$. The bulk potential $W(\Psi(z))$ attracts $\Psi_0(z)$ to one of its minima. By using at least quartic functions for W with a bifurcation of the minimum, the Landau theory is often used to describe phase transitions. Here it is sufficient to use a quadratic bulk potential,

$$W(\Psi(z))=\tfrac{1}{2}[\Psi(z)-1]^2$$

with one minimum at 1. Solving $\delta_\Psi K(\{\Psi\})|_{\Psi=\Psi_0}=0$ yields the ''equilibrium'' state parameter

$$\Psi_0(z)=1+qe^{-z/z_0}. \tag{11}$$

Combining Eq. (11) and Eq. (9) yields Eq. (4).

In the Landau model, the system can lower its free enthalpy by increasing Ψ at the surface by a factor of $(1+q)$ compared to the bulk value. This is equivalent to the increase of the atomic mobility at the surface of the MD-simulated film. Formally the increase of Ψ at the surface is induced by the additional contribution to the free enthalpy at the surface $W_s(\Psi(0))=-q\Psi(0)$. This can be understood in the MD model. The vacuum side of the surface does not hinder excursions of the surface atoms. The surface atoms have lower energy boundaries for the diffusion. The characteristic length z_0 for the transition between the surface and bulk behavior does not depend on W_s in the Landau model. z_0 is a property of the material below the surface. The model may be applied to confined glass forming liquids as well. In this case, W_s probably depends on the interaction of the surface with the confining wall. The Landau model allows the mobility at the surface to be lower than in the bulk ($q\in[-1,0]$). Note that q is limited from below to -1 corresponding to a blocked surface, but q is unlimited from above ($q\gg1$ for the free surfaces in this paper). If the interaction of the liquid with the confining wall is only of short range, the length scale z_0 of the transition between surface and bulk behavior should not depend on this interaction and should be the same as in the case of a free surface.

E. Film growth

Onto one side of the 980 K HHA-MD-simulated film (see Fig. 3), 384 additional atoms are deposited with a rate of 10 ns^{-1} at random positions and with 0.1 eV kinetic energy. In this process, Ni and Zr atoms are chosen randomly with equal probability. The resulting film growth rate amounts to 0.13 monolayers per ns. Figure 10 presents the $D(z)$ curve for this film, obtained from 10 ns recording time after the end of the deposition process. For completeness, the $D(z)$ curve of the original film is included as well. In Fig. 10, the deposited atoms were added beyond 4.2 nm film thickness. The figure indicates that the gradient in $D(z)$ remains unchanged under film growth, and that the $D(z)$ profile is shifted with the shift of the film surface. On the opposite film side, where no atoms are deposited, the gradient in $D(z)$ also remains unchanged, for $z\leqslant1$ nm. Both findings support the assumption that the gradient of $D(z)$ reflects an intrinsic property of the material at and below the film surface.

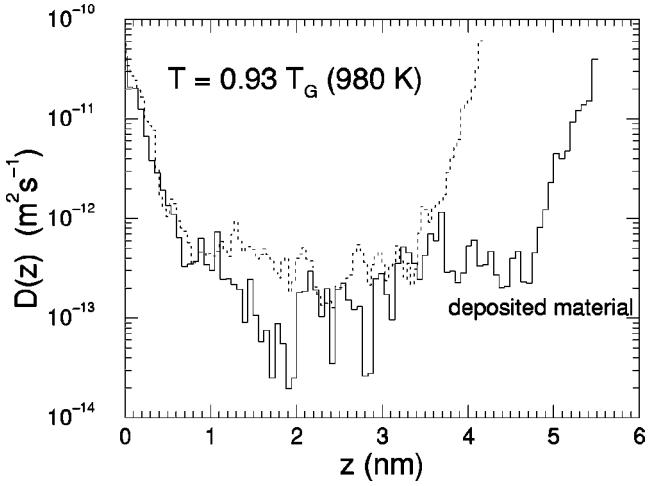

FIG. 10. Effective mean diffusion coefficients $D(z)$ in a film before and after the deposition of additional atoms onto one side of the film. As substrate serves the HHA-MD simulated amorphous $Ni_{0.5}Zr_{0.5}$ film at 980 K (dotted stair steps). The solid stair steps show the diffusion profile in the film after the deposition of 384 additional atoms. (Deposition rate: 10 ns^{-1}, kinetic energy: 0.1 eV, randomly selected Ni or Zr atoms at equal probability).

IV. SUMMARY AND DISCUSSION

MD simulations of glass forming $Ni_{0.5}Zr_{0.5}$ films have been carried out. The following scenery emerges from the results in the glass transition temperature range. The film core behaves like the simulated bulk material. Equality between the film core and the bulk material is found concerning dynamical (diffusion) and structural (angular averaged pair distribution) aspects. The mobility in the surface region is increased by about two decades. The surface retains the mobility of a supercooled liquid as the film passes the glass transition temperature range. In spite of the high mobility of the surface, an analysis of the van Hove correlations indicates a simultaneous dynamic glass transition of the whole film. A shift of the transition temperature between bulk and film is not observed. The film is homogeneous with respect to density and composition on the length scale of enhanced surface mobility.

The mobility characterized by $D(z)$ or $\nu_{NiZr}(z)$ has a constant bulk value in the core region. There is no minimum extension of this core region as seen in Fig. 5. The mobility increases exponentially from the center to the surface of the film. This profile of the mobility [Eq. (4)] in the film is consistent with a Gaussian Landau theory. In the Landau model, the length z_0 does not depend on the surface contribution to the free enthalpy. The model should also be applicable to glass forming liquids confined between smooth walls with short interatomic and liquid-wall interactions. In this case the length scale z_0 is independent of the details of the surface-wall interactions. In particular, z_0 should be the same for the confined system as for the free film. The mobility at the surface is increased by the factor $(1+q)$ in the

Landau model. q depends on the surface-wall interactions and can be different for confined and free films. q is limited from below to -1 (blocked surface).

The scale z_0 of the exponential increase changes only slightly as the film passes the glass transition temperature range. Here, the discussion about the length scales at the glass transition [19,22,25,50–53] is touched. Experiments measuring the dynamic properties of small systems yield a length at which the first deviation of the dynamic properties to those of the bulk occurs. This length can be given for a film with a diffusion following the Landau model. To estimate this thickness, we consider the total mean diffusion $\overline{D}(d)=(1/d)\int_0^d D(z)dz$ as a function of the film thickness d. For $1/d\rightarrow 0$ one finds $\overline{D}(d)/\overline{D}(\infty)=1+(d_1/d)$, where $d_1=2qz_0$. This yields only the product of z_0 and q. The length d_1 changes continuously with temperature.

In MD simulations of a metallic glass ($Pd_{0.8}Si_{0.2}$), Ballone and Rubini [54] find an enhancement of the surface dynamics by a factor of 2. This enhancement is small compared to that found in the present work. The different observations may be due to the fact that Ballone and Rubini have concentrated on large systems and relatively short time scales (some ps) while according to our experiences a relaxation over several ns is necessary to generate the here discussed mobility profiles.

The liquidlike surface might be of technical advantage for rapidly growing amorphous films by atom deposition techniques with low deposition energies (see Fig. 10), since structural inhomogeneities can easily annihilate in the mobility gradient of the surface layer. At least it should make the amorphous film growth by atom deposition techniques amenable to computer simulations. Further research concerning the temperature dependence of the enhanced mobility near the surface is in progress. In particular, the temperature range of the phenomenon and the temperature dependence of z_0 and q will be investigated.

ACKNOWLEDGMENTS

We thank the computer centers Gesellschaft für wissenschaftliche Datenverarbeitung Göttingen, Institut für wissenschaftliches Rechnen of the Technische Universität Braunschweig, Regionales Rechenzentrum Niedersachsen in Hannover, and Höchstleistungsrechenzentrum in Jülich for providing processing time on their Cray T3E parallel computers.

[1] J. W. Frenken and J. F. van der Veen, Phys. Rev. Lett. **54**, 134 (1985).
[2] R. N. Barnett and U. Landman, Phys. Rev. B **44**, 3226 (1991).
[3] A. Landa, P. Wynblatt, H. Häkkinen, R. N. Barnett, and U. Landman, Phys. Rev. B **51**, 10 972 (1995).
[4] F. Ercolessi, S. Iarlori, O. Tomagnini, E. Tosatti, and X. J. Chen, Surf. Sci. **251/252**, 645 (1991).
[5] J. S. Wettlaufer, M. G. Worster, L. A. Wilen, and J. G. Dash, Phys. Rev. Lett. **76**, 3602 (1996).
[6] J. G. Dash, H. Fu, and J. S. Wettlaufer, Rep. Prog. Phys. **58**, 115 (1995).
[7] J. Warnock, D. Awschalom, and M. Shafer, Phys. Rev. Lett. **57**, 1753 (1986).
[8] D. Awschalom and J. Warnock, Phys. Rev. B **35**, 6779 (1987).
[9] J. Drake, J. Klafter, R. Kopelman, and D. D. Awschalom, *Dynamics in Small Confining Systems*, MRS Symposia Proceedings No. 290 (Materials Research Society, Pittsburgh, 1993).
[10] J. Drake, J. Klafter, R. Kopelman, and S. Troian, *Dynamics in Small Confining Systems II*, MRS Symposia Proceedings No. 366 (Materials Research Society, Pittsburgh, 1995).
[11] J. Drake, J. Klafter, and R. Kopelman, *Dynamics in Small Confining Systems III*, MRS Symposia Proceedings No. 464 (Materials Research Society, Pittsburgh, 1997).
[12] R. Lipowsky and W. Speth, Phys. Rev. B **28**, 3983 (1983).
[13] K. Samwer, Phys. Rep. **161**, 1 (1988).
[14] R. Bormann, Mater. Sci. Eng., A **178**, 55 (1994).
[15] W. Götze and L. Sjögren, Rep. Prog. Phys. **55**, 241 (1992).
[16] D. R. MacFarlane and C. A. Angell, J. Phys. Chem. **86**, 1927 (1982).
[17] K. Hofer, E. Mayer, and G. P. Johari, J. Phys. Chem. **95**, 7100 (1991).
[18] G. Barut, P. Pissis, R. Pelster, and G. Nimtz, Phys. Rev. Lett. **80**, 3543 (1998).
[19] M. Arndt, R. Stannarius, H. Groothues, E. Hempel, and F. Kremer, Phys. Rev. Lett. **79**, 2077 (1997).
[20] C. Jackson and G. McKenna, J. Non-Cryst. Solids **131-133**, 221 (1991).
[21] J. Dubochet, M. Adrian, J. Teixeira, C. Alba, R. Kadiyala, D. MacFarlane, and C. A. Angell, J. Phys. Chem. **88**, 6727 (1984).
[22] A. L. Demirel and S. Granick, Phys. Rev. Lett. **77**, 2261 (1996).
[23] A. Huwe, M. Arndt, F. Kremer, C. Haggemüller, and P. Behrens, J. Chem. Phys. **107**, 9699 (1997).
[24] M. Arndt and F. Kremer, in *Dynamics in Small Confining Systems II*, edited by J. Drake, J. Klafter, R. Kopelman, and S. Troian, MRS Symposia Proceedings No. 366 (Materials Research Society, Pittsburgh, 1995), pp. 259–263.
[25] T. Fehr and H. Löwen, Phys. Rev. E **52**, 4016 (1995).
[26] J. L. Keddie, R. A. Jones, and R. A. Cory, Europhys. Lett. **27**, 59 (1994).
[27] J. Forrest, K. Dalnoki-Veress, J. Stevens, and J. Dutcher, Phys. Rev. Lett. **77**, 2002 (1996).
[28] G. DeMaggio, W. Frieze, D. Gidley, M. Zhu, H. Hristov, and A. Yee, Phys. Rev. Lett. **78**, 1524 (1997).
[29] Y. Jean, R. Zhang, H. Cao, J.-P. Yuan, C.-M. Huang, B. Nielsen, and P. Asoka-Kumar, Phys. Rev. B **56**, R8459 (1997).
[30] H. Teichler, Defect Diffus. Forum **143-147**, 717 (1997).
[31] C. Massobrio, V. Pontikis, and G. Martin, Phys. Rev. B **41**, 10 486 (1990).
[32] C. Hausleitner and J. Hafner, Phys. Rev. B **45**, 128 (1992).
[33] R. Devanathan, N. Q. Lam, P. R. Okamoto, M. J. Sabochick, and M. Meshii, J. Alloys Compd. **194**, 447 (1993).
[34] H. Teichler, Phys. Rev. Lett. **76**, 62 (1996).
[35] H. Teichler, Phys. Rev. E **53**, R4287 (1996).
[36] H. Teichler, Phys. Status Solidi B **172**, 325 (1992).

[37] T. Aihara, K. Aoki, and T. Masumoto, Scr. Metall. **28**, 1003 (1993).
[38] T. Aihara, K. Aoki, and T. Masumoto, Mater. Trans., JIM **36**, 399 (1995).
[39] J. T. Aihara, Y. Kawazoe, and T. Masumoto, Mater. Trans., JIM **36**, 835 (1995).
[40] J. T. Aihara, Y. Kawazoe, and T. Masumoto, Sci. Rep. Res. Inst. Tohoku Univ. A **42**, 57 (1996).
[41] Z. Altounian, G.-H. Tu, and J. O. Strom-Olsen, J. Appl. Phys. **54**, 3111 (1983).
[42] J. Eckert, L. Schultz, and K. Urban, J. Mater. Res. **6**, 1874 (1991).
[43] J. R. Gachon, M. Dirand, and J. Hertz, J. Less-Comm. Metals **92**, 307 (1983).
[44] C. Hausleitner and J. Hafner, Phys. Rev. B **45**, 115 (1992).
[45] M. W. Finnis, J. Phys. F **4**, 1645 (1974).
[46] M. Spangenberg, diploma thesis, Universität Göttingen, 1997.
[47] D. J. Oh and R. A. Johnson, J. Mater. Res. **3**, 471 (1988); D. J. Oh and R. A. Johnson, in *Atomistic Scale Simulations of Materials—Beyond Pair Potentials*, edited by V. Vitek and D. Srolovitz (Plenum, New York, 1989).
[48] R. S. Averback, Mater. Res. Bull. **16**, 47 (1991).
[49] R. Lipowsky and W. Speth, Phys. Rev. B **28**, 3983 (1983).
[50] L. Bocquet and J.-L. Barrat, Europhys. Lett. **31**, 455 (1995).
[51] E. Fischer, E. Donth, and W. Steffen, Phys. Rev. Lett. **68**, 2344 (1992).
[52] W. Kob, C. Donati, S. J. Plimpton, P. H. Poole, and S. C. Glotzer, Phys. Rev. Lett. **79**, 2827 (1997).
[53] D. Sappelt and J. Jäckle, J. Phys. A **26**, 7325 (1993).
[54] P. Ballone and S. Rubini, Surf. Sci. **342**, L1116 (1995).